Constraining the Einstein-dilaton-Gauss-Bonnet theory with higher harmonics and the merger-ringdown contribution using GWTC-3

Baoxiang Wang, Changfu Shi,* Jian-dong Zhang, Yi-Ming Hu, and Jianwei Mei

MOE Key Laboratory of TianQin Mission, TianQin Research Center for Gravitational Physics and School of Physics and Astronomy, Frontiers Science Center for TianQin, Gravitational Wave Research Center of CNSA, Sun Yat-sen University (Zhuhai Campus), Zhuhai 519082, China

(Received 23 February 2023; accepted 7 August 2023; published 25 August 2023)

In this paper, we revisit the problem of using gravitational wave data to test the Einstein-dilation-Gauss-Bonnet theory by using nine selected gravitational wave events from the third Gravitational-Wave Transient Catalog. Compared with existing work, we take into account the higher harmonics more properly and we also study the contribution of the merger-ringdown data. Using the inspiral data alone, we find that the best result is from GW200115, giving $\sqrt{|\alpha|} < 1.1$ km, which is about 17% tighter than the previous best result. Several combinations of the selected events give $\sqrt{|\alpha|} \leq 1.0$ km. The result is further improved when the merger-ringdown data are also included, using two phenomenological schemes, giving $\sqrt{|\alpha|} < 0.87$ km for GW200115 in the best case scenario. We also notice the possible existence of a simple unexpected relation among the constraints from different events, and it is important to have more large mass ratio events that can help clarify if there is indeed such a trend.

DOI: 10.1103/PhysRevD.108.044061

I. INTRODUCTION

The detection of gravitational waves (GWs) from compact binaries has opened the door to study the nature of gravity and dark compact objects in the genuinely strong field and dynamical regime. By using the currently available GW data [1–5], a variety of tests have been performed [6–16]. For example, there have been theory agnostic tests, such as residual tests [6], inspiral-merger-ringdown consistency tests [17], and searches for possible deviations from the post-Newtonian (PN) waveform [18]; there have been tests on specific topics, such as the no-hair theorem [19], GW polarization [20], graviton mass [6], the spin-induced quadrupole moment [21], the GW dispersion relation [22], extra dimension [16], time-varying gravitational constant G(t) [23], and the gravitational Lorentz invariance [24]. There have also been tests targeting different modified gravity (MG) theories [11–16,25–34]. No evidence against general relativity (GR) has been found so far.

For the existing tests, the full inspiral-merger-ringdown data have been used in the residual test, the inspiral-merger-ringdown consistency test, and the polarization test, while the test on the no-hair theorem only uses the ringdown data, and tests on the PN waveform, the spin-induced quadrupole moment, and almost all theory-/topic-specific tests only use the inspiral data. What is more, previous works using the inspiral data have only considered corrections to the dominant 22 mode or have assumed a universal correction for all harmonics. For some tests, especially the theory-specific tests, it is natural to expect that both the higher harmonics and the merger-ringdown data can make a difference. However, taking these factors into consideration has to come supported with adequate waveform modeling in the theories being tested. A good example here is the test of the Einstein-dilaton-Gauss-Bonnet (EdGB) theory [35–38].

EdGB is a quantum gravity-inspired modified gravity theory featuring a dilation coupled to the Gauss-Bonnet invariant, through a dimensionful coupling constant α. Since the coupling is dimensionful, one generally expects the constraint to be of the order $\sqrt{|\alpha|} < \mathcal{O}(L)$, where L is the typical curvature radius of the system under consideration [39]. Indeed, electromagnetic observation of the orbital decay of black hole low mass x-ray binary A0620-00 has produced a constraint $\sqrt{|\alpha|} < 1.9$ km [38], which is of the expected order.

Black hole binaries in EdGB generically have dipolar GW emission and so the theory is expected to get strong constraints with GWs [40], and a series of studies on inspiral waveform in this theory have been conducted [40–45]. The first estimation of the constraints on EdGB with real GW source information has been done using the Fisher information matrix (FIM) method [16]. The amplitude correction to the waveform was later included but the calculation was still FIM based [46]. The full Bayesian

*Corresponding author: shichf6@mail.sysu.edu.cn

analysis of EdGB was first performed with the first Gravitational-Wave Transient Catalog (GWTC-1) data in [47] and then with GWTC-2 data in [11]. Both works have selected events with small mass ratios (defined to be the major mass over the minor mass). However, systems with larger mass ratios tend to place stronger constraints on α [40,41,48]. For such systems, significant contributions from higher harmonics are expected. The contribution of higher harmonics has been considered in [12,49] with large mass ratio events such as GW190814, but only (2, 2) mode EdGB correction has been considered. Recently, a parametrized post-Einsteinian (ppE) waveform model has been constructed in which the relations among the corrections to different harmonics have been carefully calculated [50].

Including the merger-ringdown data in theory-specific tests is challenging due to the difficulties with numerical relativity simulation [51–53] and quasinormal mode (QNM) [54–59] calculation in the corresponding MG theories. For EdGB, a test with inspiral and ringdown data has been carried out based on QNMs found in a spherically symmetric background [60,61]. For more general situations, several schemes have recently been proposed [62] to model phase corrections beyond the inspiral stage, based on the structure of IMRPhenomD waveforms [63,64].

In this paper, we revisit the problem of testing EdGB with real GW data. We refine over existing work in the following ways:

(i) We apply the work of [50] to EdGB and obtain a waveform model containing the correct relation among the corrections to different harmonics. To apply the result of [50], we need to use waveform models that assume nonprecessing binaries; for this we will use the IMRPhenomXHM waveform [65].
(ii) We apply the method of [62] to the IMRPhenomXHM waveform so that the merger-ringdown data can also be used.
(iii) We have included a couple of new events from GWTC-3 that have never been used to test EdGB before.

We find that (i) the appropriate inclusion of higher harmonic modes can make appreciable difference in the result. For example, there can be about 50% improvement on the results from GW190707, GW190720, and GW190728 over previous ones that do not include higher harmonics [11], and there can be nearly 30% improvement from GW190421 compared to the previous result that assumes a universal correction for all higher harmonics [12]. (ii) All constraints from the selected GW events seem to be closely distributed by the line described by (18) below. (iii) The effect of merger-ringdown data is relatively less significant, but can still give about 20% improvement for GW200115, compared to that without using the merger-ringdown data. (iv) Our best constraint comes from GW200115, which with higher harmonic modes alone gives $\sqrt{|\alpha|} < 1.1$ km, and if the merger-ringdown data are also taken into account, it gives $\sqrt{|\alpha|} < 0.87$ km. As a comparison, the current best constraint on EdGB comes from [49], which also uses GW200115, giving $\sqrt{|\alpha|} < 1.33$ km.

This paper is organized as follows. We introduce how the higher harmonics and the merger-ringdown contribution are included into the waveform model in Sec. II, select the GW events to be used and make necessary explanations of the statistical method in Sec. III, present the main results in Sec. IV, and then make short concluding remarks in Sec. V.

We use the convention $G = c = 1$ throughout the paper.

II. WAVEFORM MODELS

In this section, we explain the construction of the waveform models used in this paper.

A. The ppE waveform model with higher harmonic contributions

The evolution of compact binaries is divided into three stages: inspiral, merger, and ringdown. During the inspiral stage, the binary components are widely separated, their velocities are relatively small, and the PN approximation [66] can be used to obtain the waveforms for low mass ratio systems. The ppE waveform model has been proposed to capture the common features of how the PN waveforms in many MG theories deviate from those in GR [67]. Keeping only the leading order correction, the inspiral waveform for an MG theory can be written as

$$\tilde{h}_{\rm ppE}(f) = \tilde{h}_{\rm GR}(f)(1 + \alpha u^a)e^{i\beta u^b}, \tag{1}$$

where α and β are the ppE parameters, $b = 2\mathrm{PN} - 5$ and $a = b + 5$ are the ppE order parameters, and the PN in this equation symbolizes the PN order. $u = (\pi\mathcal{M}f)^{1/3}$ is a characteristic velocity, $\mathcal{M} = \eta^{3/5}M$ is the chirp mass, $M = m_1 + m_2$ is the total mass, $\eta = m_1 m_2/(m_1 + m_2)^2$ is the symmetrical mass ratio, m_1 and m_2 are the major and minor masses, respectively, and $h_{\rm GR}$ is the corresponding GR waveform.

To take into account the contribution of higher harmonics, the construction of [50] neglects the contribution of the amplitude correction, leading to

$$\tilde{h}_{\rm ppE}(f) = \tilde{h}_{\rm GR}(f)e^{i\beta u^b}. \tag{2}$$

The error introduced in this process is expected to be less than a few percent [46]. Early works [11,47] using GWTC-1 and GWTC-2 data to test EdGB have only considered the 22 mode of $\tilde{h}_{\rm GR}$ in (2), while the authors of [12,49] have considered the contribution of higher harmonics, but have assumed only the 22 mode EdGB correction, i.e.,

$$\tilde{h}_{\rm ppE}(f) = \left[\sum_{\ell m}\tilde{h}^{\rm GR}_{\ell m}(f)\right]e^{i\beta_{22}u^{b_{22}}}. \tag{3}$$

It should be noticed that the contributions of higher post-Newtonian order corrections up to 2 PN have been considered in [49]. However, there is no reason to believe that the ppE corrections to all the higher harmonics are zero, and one would naturally expect

$$\tilde{h}_{\rm ppE}(f) = \sum_{\ell m} \tilde{h}^{\rm ppE}_{\ell m}(f),$$
$$\tilde{h}^{\rm ppE}_{\ell m}(f) = \tilde{h}^{\rm GR}_{\ell m}(f) e^{i\beta_{\ell m} u^{b_{\ell m}}}, \tag{4}$$

where both $\beta_{\ell m}$ and $b_{\ell m}$ can be different for different values of ℓ and m. Indeed, it has been found that [50]

$$\beta_{\ell m} = \left(\frac{2}{m}\right)^{b/3-1} \beta_{22}, \qquad b_{\ell m} = b_{22}. \tag{5}$$

In this paper, the GR waveform will be produced using IMRPhenomXHM, and the higher harmonics modes $(\ell, |m|) = \{(2,2),(2,1),(3,3),(3,2),(4,4)\}$ are considered.

Given an MG theory, the relation between the ppE parameters and the theory parameters can be established by calculating corrections to binary orbits [41].

B. EdGB theory

The EdGB is a quantum gravity-inspired modified gravity theory; it introduces a dilation coupled to the Gauss-Bonnet invariant. The action of this theory can be written as follows:

$$S = \int d^4x\sqrt{-g}\left[\frac{R}{16\pi} - \frac{(\nabla\phi)2}{2} + \alpha\phi\mathcal{R}_{\rm GB}\right] + S_m, \tag{6}$$

where $\mathcal{R}_{\rm GB} = R^2 - 4R_{\mu\nu}R^{\mu\nu} + R_{\mu\nu\sigma\rho}R^{\mu\nu\sigma\rho}$ is the Gauss-Bonnet invariant, R and $R_{\mu\nu}$ are the Ricci scalar and Ricci tensor, respectively, and g is the determinant of the metric $g_{\mu\nu}$. ϕ is a massless scalar field and α is the coupling constant with the unit of $(\text{length})^2$. S_m is the matter action.

The leading order modification in the GW waveform introduced by EdGB theory starts at the -1PN order, corresponding to $b_{22} = -7$, and it has been found that [40]

$$\beta_{22} = -\frac{5\zeta}{7168}\frac{(m_1^2\tilde{s}_2 - m_2^2\tilde{s}_1)^2}{M^4\eta^{18/5}}, \tag{7}$$

where $\zeta \equiv 16\pi\alpha^2/M^4$ [35], and $\tilde{s}_n$, $n = 1, 2$, is the scalar charge for the nth component. If the component is a black hole, we have $\tilde{s}_n \equiv 2(\sqrt{1-\chi_n^2} - 1 + \chi_n^2)/\chi_n^2$, and χ_n is the spin of the nth component. If it is a neutron star, the corresponding scalar charge is zero.

The current waveform of EdGB, i.e., Eq. (7), is derived in the small-coupling limit, and we assume that the EdGB corrections can be regarded as small perturbations compared with GR contributions. Following the choices in [11,47–49], a rough threshold for the coupling constant has to satisfy the bound

$$\alpha^2 \simeq \frac{m_2^4}{32\pi}, \tag{8}$$

where m_2 is the mass of the minor black hole component. If the system is a black hole binary (BHB), m_2 is the mass of the minor component. However, if the system is a neutron star–black hole binary (NSBH), m_2 is the mass of the black hole component.

C. Waveform model for the merger-ringdown stage

Although it is tempting to use all the available GW data to test a given MG theory, such as EdGB, there still lacks a good waveform model that properly takes into account the corresponding MG correction at the merger and ringdown stages, due to the difficulty with numerical relativity simulation [51–53] and QNM calculations [54–59].

In this paper, we will follow [62] and use the following phenomenologically motivated waveforms for the merger and ringdown stages:

(i) Zero correction: This is the simplest case when no contribution from the merger-ringdown stage is invoked,

$$\tilde{h}^{\rm Zero}_{\ell m}(f) = \begin{cases} \tilde{h}^{\rm GR}_{\ell m}(f) e^{i\beta_{\ell m} u^{b_{\ell m}}}, & f < f^{\rm IM}_{\ell m}, \\ 0, & f \geq f^{\rm IM}_{\ell m}, \end{cases} \tag{9}$$

where $f^{\rm IM}_{\ell m}$ is the GW frequency when the binary system reaches its minimal energy circular orbit as defined in [68], i.e., $Mf^{22}_{\rm IM} = 0.014$ and $f^{\ell m}_{\rm IM} = \frac{m}{2} f^{22}_{\rm IM}$ for IMRPhenomXHM [65].

(ii) C^0 correction: In this case, the correction in the merger-ringdown stage is modeled with a fixed phase,

$$\tilde{h}^{\rm C^0}_{\ell m}(f) = \begin{cases} \tilde{h}^{\rm GR}_{\ell m} e^{i\beta_{\ell m} u^{b_{\ell m}}}, & f < f^{\rm IM}_{\ell m}, \\ \tilde{h}^{\rm GR}_{\ell m} e^{i\beta_{\ell m} u^{b_{\ell m}}_{\rm IM}}, & f \geq f^{\rm IM}_{\ell m}, \end{cases} \tag{10}$$

where $u_{\rm IM} = (\pi\mathcal{M}f^{\rm IM}_{\ell m})^{1/3}$. This waveform indicates that no more correction information will be integrated during the merger-ringdown stage.

(iii) C^∞ correction: In this case, the form of correction in the inspiral stage is carried all the way through the merger-ringdown stages,

$$\tilde{h}^{\rm C^\infty}_{\ell m}(f) = \tilde{h}^{\rm GR}_{\ell m} e^{i\beta_{\ell m} u^{b_{\ell m}}}. \tag{11}$$

Unlike the zero correction, Eq. (9), this waveform applies the phase correction $e^{i\beta u^b}$ across the entire frequency band, including the merger-ringdown stages.

It should be noted that these three phenomenological parametrized waveforms for the merger-ringdown stages may be somewhat sketchy when one focuses on any specific MG theories. Especially, the quasinormal modes of any black holes in specific MG theory should deviate from the prediction of GR, which would introduce additional phase correction for the ringdown stage, and there is no reason for the correction to be consistent with the form of inspiral. Typical examples are the calculations of the axial and polar quasinormal modes in EdGB [59,60]; those results are incompatible with any of the three parametrized forms. Whereas the C^0 correction and C^∞ correction could also provide some insight into the importance of merger-ringdown data.

III. DATA SOURCE AND DATA ANALYSIS METHODS

In this section, we explain how the GW events are selected and clarify the specifics of the statistical method used in this paper.

A. Selection of GW events

There are 90 GW events in the current GWTC-3 catalog [5], and using all of them to test EdGB would be too expensive for computation, so it is preferable to choose a limited number of events that can put EdGB under the most stringent test. As guidance for selecting the events, we would like to have reliable and strong events that have low false alarm rate (FAR) (i.e., FAR $< 10^{-3}$ yr^{-1}) and high signal-to-noise ratio (SNR) (i.e., SNR > 10), and we also want events that have low total mass but large mass ratio. We are thus led to the set of GW events listed in Table I, guided mainly by the requirement on SNR, total mass, and mass ratio. For later use, we also list the mass, denoted as M_*, of the smallest black hole involved in each GW event.[1] It turns out that all these events have a FAR $< 10^{-5}$ yr^{-1}. We will consider two possibilities for GW190814: one as a NSBH, denoted as GW190814^a, and one as a BHB, denoted as GW190814^b. The selected events can be roughly divided into two groups:

(i) High mass ratio events with $q \geq 3$.
(ii) Low mass ratio events with $3 > q \geq 1$.

One can see that only three events belong to the high mass ratio group. For events in the high mass ratio group, constraints on EdGB with higher harmonics contribution have been studied before [12,49], while for events in the low mass ratio group, no higher harmonic contribution has been considered [11].

[1]If the system is a BHB, then M_* is the mass of the minor component, but if the system is a NSBH, then M_* is the mass of the black hole.

TABLE I. The list of selected GW events. $M_*(M_\odot)$ is the mass of the smallest black hole involved in each event.

Designation	$M(M_\odot)$	$M_*(M_\odot)$	q	SNR
GW190412	36.8	9.0	3.08	19.8
GW190814^a	25.9	23.3	8.96	25.3
GW190814^b	25.9	2.6	8.96	25.3
GW200115	7.4	5.9	4.1	11.3
GW190707	20.1	7.9	1.53	13.1
GW190720	21.8	7.5	1.89	10.9
GW190728	20.7	8.0	1.56	13.1
GW190924	13.9	5.1	1.73	12.0
GW191129	17.5	6.7	1.6	13.1
GW200202	17.6	7.3	1.38	10.8

B. Bayesian inference

The statistics are done with Bayesian inference. According to Bayes theorem, given the data d and hypothesis H, the posterior probability distribution of a set of parameters θ is given by

$$p(\theta|d,H) = \frac{p(d|\theta,H)\pi(\theta|H)}{\mathcal{Z}(d|H)}, \tag{12}$$

where $p(d|\theta,H)$ and $\pi(\theta|H)$ are the likelihood and prior, respectively. The evidence $\mathcal{Z}(d|H)$ is an overall normalization and will not be used in our calculation.

The GW and theory parameters used in this work are listed in Table II. Note that χ_1 and χ_2 are dimensionless and the spins are assumed to be aligned with the orbital angular momentum. Assuming stationary and Gaussian noise, the likelihood can be written as

$$p(d|\theta,H) \propto \exp\left[-\frac{1}{2}\sum_{j=1}^{N}(d_j - h_j|d_j - h_j)\right], \tag{13}$$

where the inner product is defined as [69]

TABLE II. GW and theory parameters involved in this study.

Symbol	Physical meaning
m_1	Mass of the major component
m_2	Mass of the minor component
χ_1	Spin of the major component
χ_2	Spin of the minor component
α_S	Right ascension of source location
δ	Declination of the source location
ψ	Polarization angle
ι	Inclination angle
$\phi_{\rm ref}$	Phase at the reference frequency
t_c	Coalescence time
D_L	Luminosity distance
$\sqrt{\lvert\alpha\rvert}$	Parameter from the EdGB coupling

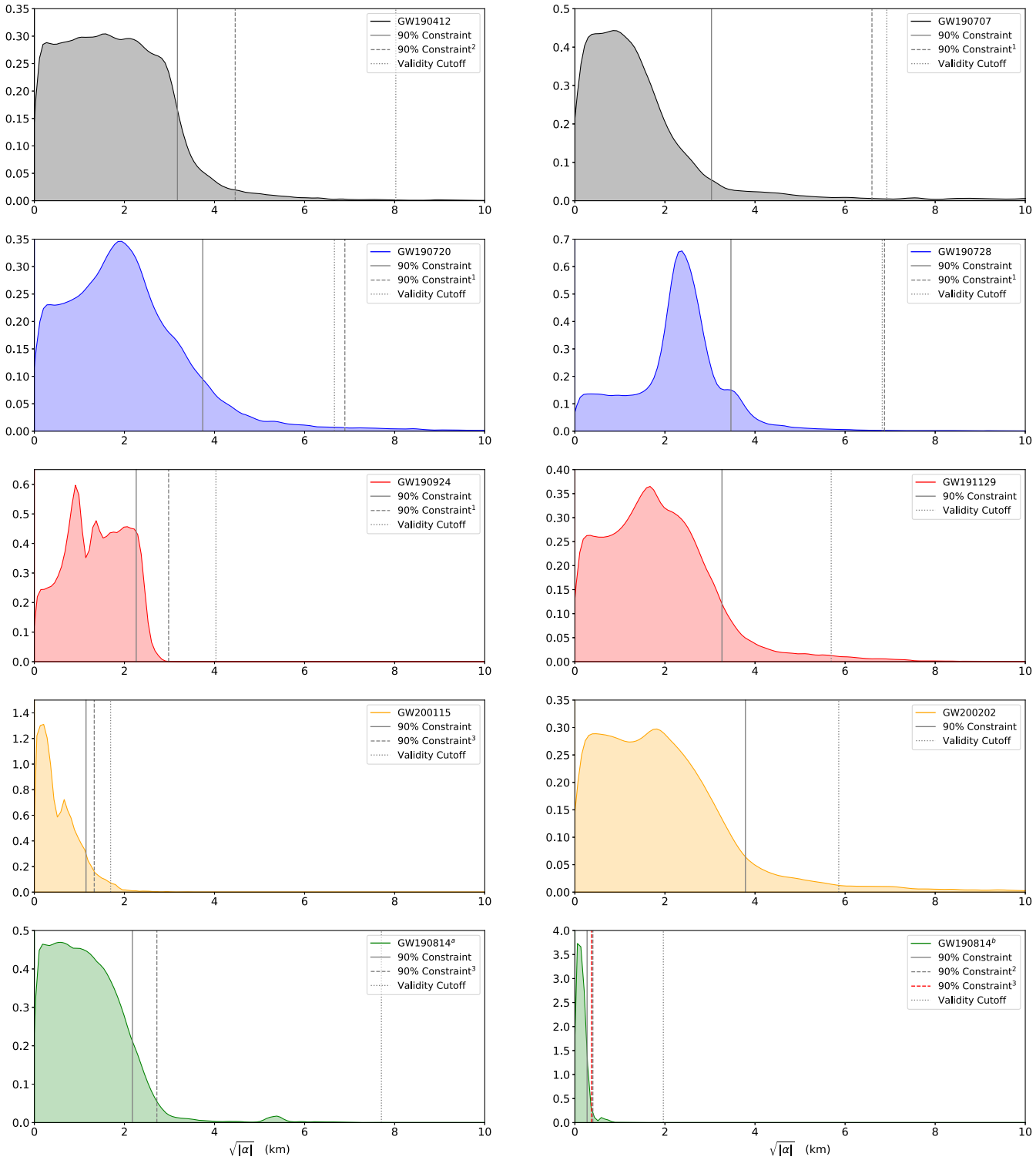

FIG. 1. The cumulative posterior distributions for $\sqrt{|\alpha|}$ obtained with the inspiral data of selected GW events. In each panel, the solid vertical line stands for the constraint on $\sqrt{|\alpha|}$ with 90% probability; the dashed vertical line stands for existing results from the literature. The superscripts 1, 2, and 3 correspond to Refs. [11,12,49], respectively, and the corresponding values are also listed in Table III. The dotted vertical line stands for the location where the weak coupling limit, characterized by $\alpha^2 \lesssim \frac{m_2^4}{32\pi}$ [11,49], is saturated, and above which the results are no longer reliable.

$$(x|y) = 2\int_{f_{\rm low}}^{f_{\rm high}} \frac{\tilde{x}^*(f)\tilde{y}(f) + \tilde{x}(f)\tilde{y}^*(f)}{S_n(f)}\,df. \quad (14)$$

Here $\tilde{x}^*$ means the complex conjugate of the Fourier component of x, $S_n(f)$ is the power spectral density of the detector, and $f_{\rm low}$ and $f_{\rm high}$ are the frequency bounds. We assume the prior to be uniform for m_1, m_2, χ_1, χ_2, $\phi_{\rm ref}$, and t_c, the events are spatially uniformly distributed, and $\sqrt{|\alpha|}$ is uniform in [0, 15] km.

We have used the PyCBC package [70] to do the Bayesian inference, and the Markov chain Monte Carlo sampling is done with the EMCEE_PT sampler [71]. We use 32 s of data for all the events selected and set $f_{\rm low} = 20$ Hz.

IV. RESULTS

In this section, we present the main findings of this work.

A. Constraints from the inspiral stage

Existing GW constraints on EdGB have been obtained only using the inspiral data. The contribution of higher harmonics has been considered in [12,49], but only the 22 mode EdGB correction has been considered. Here we revisit the problem by using the corrected waveform model (4), which has been obtained in [50] recently. An independent Bayesian inference has been carried out for each GW source listed in Table I, except that GW190814 has been used twice, first as a NSBH and then as a BHB.

The posterior distribution of $\sqrt{|\alpha|}$ is obtained by marginalizing over all other parameters and the results are plotted in Fig. 1. The corresponding 90% constraints are listed in Table III. One can see that all the selected GW events can constrain $\sqrt{|\alpha|}$ to better than about 4 km.

TABLE III. 90% constraints on $\sqrt{|\alpha|}$ using the inspiral data from selected GW events.

GW event	90% Constraint	Existing result	Improvement (%)
GW190412	3.18	4.46 [12]	29
GW190814^a	2.18	2.72 [49]	20
GW190814^b	0.27	0.4 [12]	32
		0.37 [49]	25
GW200115	1.1	1.33 [49]	17
GW190707	3.03	6.59 [11]	54
GW190720	3.74	6.90 [11]	46
GW190728	3.47	6.87 [11]	50
GW190924	2.26	2.98 [11]	24
GW191129	3.27	...	...
GW200202	3.79	...	...
Combination 1	1.00	...	...
Combination 2	0.25	...	...
Combination 3	0.98	...	...

The strongest constraint comes from GW190814^b, giving $\sqrt{|\alpha|} < 0.27$ km, which is about 25% improvement over the previous results that have taken higher harmonics into consideration [12,49]. If GW190814 is not a BHB, then the strongest constraint comes from GW200115, giving $\sqrt{|\alpha|} < 1.1$ km, which is about 17% improvement over the existing result [49]. Except for GW190814^b, the strongest constraint obtained from a BHB event comes from GW190924, which gives $\sqrt{|\alpha|} < 2.26$ km.

We also calculated the scenario where only the leading order of the 22 mode EdGB correction is considered, using GW190814^a, GW190814^b, and GW200115, in order to assess the reliability of our results. All of the settings for the Bayes inference remain the same with the scenario where higher harmonics are under consideration. The corresponding 90% constraints are 3.0, 0.39, and 1.4 km. It should be noted that [12] mentions a similar result concerning GW190814^b, but with the use of a different GR waveform, the 90% constraint derived from their results is 0.4 km. It should also be noted that the improvement brought by higher harmonics correction is about 27%, 30%, and 21% for GW190814^a, GW190814^b, and GW200115, respectively, compared to the case with only 22 mode corrections considered. From the point of view of the Fisher information matrix method [48,69], the parameter estimation accuracy of α with higher harmonic EdGB correction can be written as

$$\delta\alpha^2 \simeq \sqrt{\Gamma^{-1}_{\alpha^2\alpha^2}} = \left(\frac{\partial\tilde{h}_{\rm ppE}}{\partial\alpha^2}\middle|\frac{\partial\tilde{h}_{\rm ppE}}{\partial\alpha^2}\right)^{-1/2}, \quad (15)$$

where $\Gamma_{\rho\sigma} \equiv (\frac{\partial h}{\partial\rho}|\frac{\partial h}{\partial\sigma})$ is the Fisher information matrix, and $(|)$ donates the inner product. According to Eqs. (4) and (5), one can infer that

$$\frac{\partial\tilde{h}_{\rm ppE}}{\partial\alpha^2} = \sum_{\ell m}\tilde{h}^{\rm GR}_{\ell m}u^b\left(\frac{2}{m}\right)^{-\frac{10}{3}}\frac{\partial\beta_{22}}{\partial\alpha^2}. \quad (16)$$

For the specific case of the IMRPhenomXHM waveform, Eq. (15) can be written as

$$\delta\alpha^2 \simeq \left(1 + 2^{\frac{-10}{3}}\frac{\tilde{h}^{\rm GR}_{21}}{\tilde{h}^{\rm GR}_{22}} + \left(\frac{2}{3}\right)^{\frac{-10}{3}}\frac{\tilde{h}^{\rm GR}_{33}}{\tilde{h}^{\rm GR}_{22}} + \frac{\tilde{h}^{\rm GR}_{32}}{\tilde{h}^{\rm GR}_{22}} + \left(\frac{1}{2}\right)^{\frac{-10}{3}}\frac{\tilde{h}^{\rm GR}_{44}}{\tilde{h}^{\rm GR}_{22}}\right)^{-1} \times \left(\frac{\partial\tilde{h}^{\rm ppE}_{22}}{\partial\alpha^2}\middle|\frac{\partial\tilde{h}^{\rm ppE}_{22}}{\partial\alpha^2}\right)^{-1/2}. \quad (17)$$

One can conclude that the contributions of h_{33} and h_{44} are significant, and the improvements introduced by higher harmonic correction, i.e., $(\delta\sqrt{\alpha}_{22} - \delta\sqrt{\alpha})/\delta\sqrt{\alpha}_{22}$, are about 23% and 28% for the binary with $q = 4.1$ and $q = 8.96$, respectively, compared to the case with only 22 mode correction considered. These improvements are

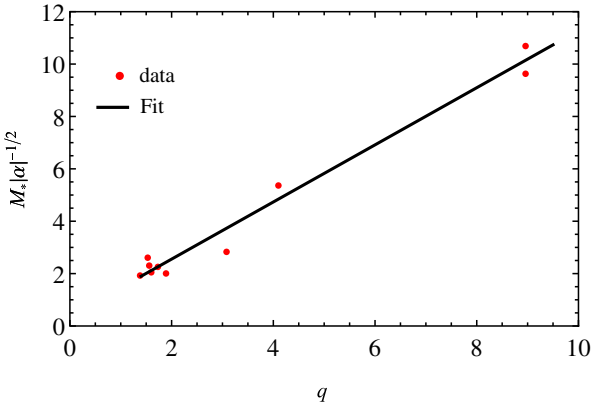

FIG. 2. The distribution of constraints from different events.

basically in good agreement with the results of our Bayesian analysis.

An inspection of Tables I and III suggests that there might be some simple approximate relation among the constraints and the parameters of different events; we are thus led to produce the plot given in Fig. 2. One can see that all the constraints found in Table III are distributed not far away from the line,

$$\frac{M_*}{\sqrt{|\alpha|}} \approx 0.37 + 1.1q. \tag{18}$$

We do not know a reason that could lead to such a simple relation and we think more data (especially those with large mass ratios) will help clarify if there is indeed such a trend.

We also obtain combined constraints on $\sqrt{|\alpha|}$ by superimposing the posteriors of individual events [6]. Three combinations have been considered:

(i) Combination 1: Including all single events in Table III, but not GW190814^a or GW190814^b.
(ii) Combination 2: Including all single events in Table III, but not GW190814^a.
(iii) Combination 3: Including all single events in Table III, but not GW190814^b.

One can see that the constraints can reach 1 km or better for all three combinations.

B. The effect of the merger-ringdown data

Here we use the best events from the last subsection, GW190814^b, GW190924, and GW200115, all of which are characterized by containing a very low mass black hole, to study the contribution of merger-ringdown data. We also present the results on GW190814^a just to make the study of this event more complete.

The results are plotted in Fig. 3 and the corresponding 90% constraints are listed in Table IV. For the four cases studied, we see that the posterior distributions of C^0 and C^∞ corrections can be appreciably different from that of

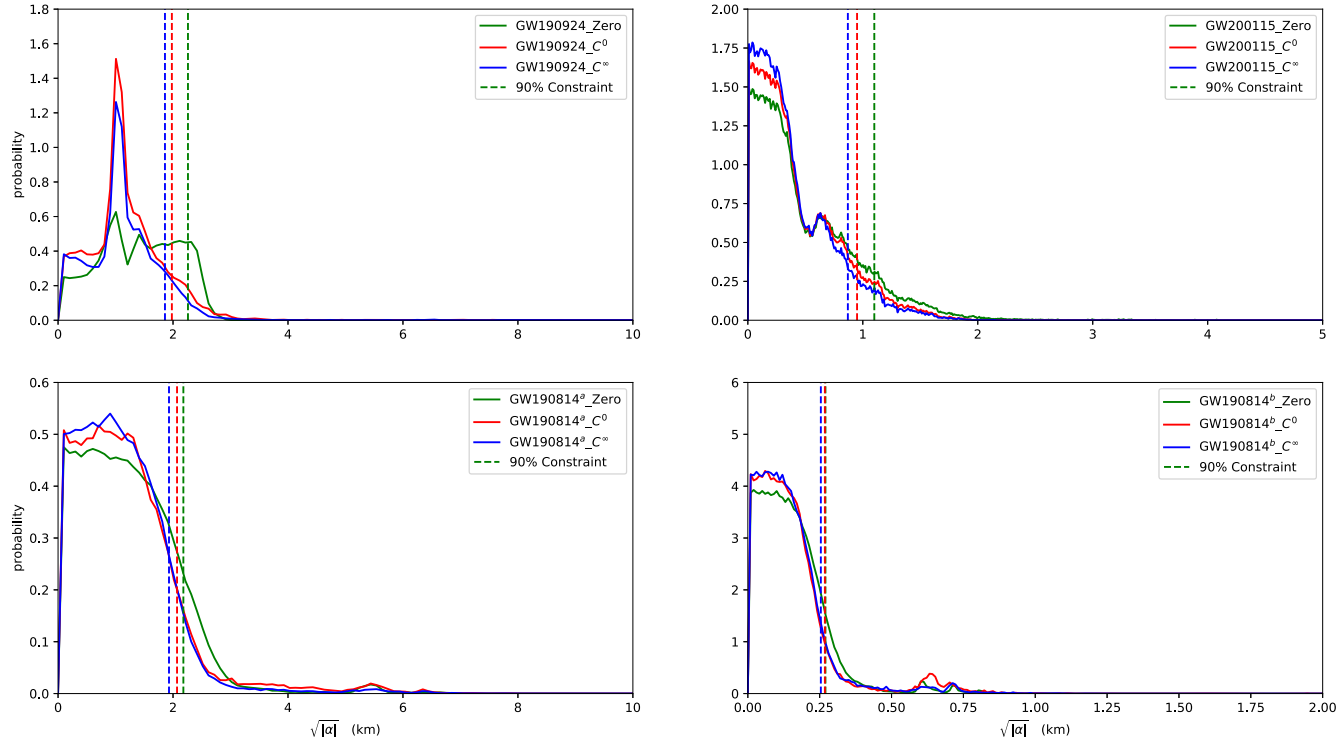

FIG. 3. The cumulative posterior distributions for $\sqrt{|\alpha|}$ obtained with the full inspiral-merger-ringdown data using selected GW events.

TABLE IV. Constraints on $\sqrt{|\alpha|}$ with merger-ringdown contributions. The percentage values in the lines of C^0 and C^∞ stand for the improvement made compared to the case of zero correction.

	GW190814			
GW events	BHB	NSBH	GW190924	GW200115
Zero correction	0.27	2.18	2.26	1.10
C^0	0.268	2.07	1.98	0.95
	0.7%	5%	12.4%	13.6%
C^∞	0.254	1.93	1.86	0.87
	5.9%	11.5%	17.7%	20.9%

zero correction, while the difference between C^0 and C^∞ corrections is relatively less significant. One can also see that the merger-ringdown part can make an appreciable correction to the constraints, reaching as large as 20% for the cases studied in this paper.

V. CONCLUSION

In this paper, we have revisited the problem of constraining EdGB with real GW data. We have selected nine events from GWTC-3 [72] and have paid particular attention to properly include the higher harmonics in the waveform model for the inspiral stage and have considered two schemes to include the contribution of the merger-ringdown data.

We find that different ways to include the higher harmonics can make a significant difference in the resulting constraints. For example, for some of the low mass ratio sources, such as GW190707 and GW190728, for which the higher harmonics have never been used to constrain EdGB in previous studies, we find that the improvement can be as large as 50%. For the high mass ratio events, for which the higher harmonics have already been considered in previous studies, but by using the correct relation among the corrections to different harmonics [50], one can still get improved results. In the case of GW190412, for example, the improvement can be as large as 29%.

We also find that the most stringent constraint comes from the events that contain the least massive black holes. In particular, all constraints from the selected GW events seem to be closely distributed by the line (18). This is consistent with the expectation that the constraint on $\sqrt{|\alpha|}$ is at the order of the typical curvature radius of the system [39]. We stress the importance of having more large mass ratio events, which are expected to help clarify if there is indeed such a trend.

We also considered two schemes to include the merger-ringdown data in the test. By using the GW events that pose to give the most stringent constraint on EdGB, we find that the contribution from the merger-ringdown stage can improve the constraint by as large as about 20%.

ACKNOWLEDGMENTS

The authors thank Yi-Fan Wang for useful discussions and Alexander Harvey Nitz for the helpful communication on the use of PyCBC. This work has been supported by the Guangdong Basic and Applied Basic Research Foundation (Grant No. 2021A1515010319), the Guangdong Major Project of Basic and Applied Basic Research (Grant No. 2019B030302001), and the Natural Science Foundation of China (Grant No. 12173104).

[1] B. P. Abbott *et al.* (LIGO Scientific and Virgo Collaborations), Phys. Rev. Lett. **116**, 061102 (2016).
[2] B. P. Abbott *et al.* (LIGO Scientific and Virgo Collaborations), Phys. Rev. X **9**, 031040 (2019).
[3] R. Abbott *et al.* (LIGO Scientific and Virgo Collaborations), Phys. Rev. X **11**, 021053 (2021).
[4] R. Abbott *et al.* (LIGO Scientific and Virgo Collaborations), arXiv:2108.01045.
[5] R. Abbott *et al.* (LIGO Scientific, VIRGO, and KAGRA Collaborations), arXiv:2111.03606.
[6] B. P. Abbott *et al.* (LIGO Scientific and Virgo Collaborations), Phys. Rev. Lett. **116**, 221101 (2016); **121**, 129902(E) (2018).
[7] B. P. Abbott *et al.* (LIGO Scientific and Virgo Collaborations), Phys. Rev. Lett. **123**, 011102 (2019).
[8] B. P. Abbott *et al.* (LIGO Scientific and Virgo Collaborations), Phys. Rev. D **100**, 104036 (2019).
[9] R. Abbott *et al.* (LIGO Scientific and Virgo Collaborations), Phys. Rev. D **103**, 122002 (2021).
[10] R. Abbott *et al.* (LIGO Scientific, VIRGO, and KAGRA Collaborations), arXiv:2112.06861.
[11] S. E. Perkins, R. Nair, H. O. Silva, and N. Yunes, Phys. Rev. D **104**, 024060 (2021).
[12] H.-T. Wang, S.-P. Tang, P.-C. Li, M.-Z. Han, and Y.-Z. Fan, Phys. Rev. D **104**, 024015 (2021).
[13] R. Niu, X. Zhang, B. Wang, and W. Zhao, Astrophys. J. **921**, 149 (2021).
[14] Z. Wang, L. Shao, and C. Liu, Astrophys. J. **921**, 158 (2021).
[15] A. Kobakhidze, C. Lagger, and A. Manning, Phys. Rev. D **94**, 064033 (2016).
[16] N. Yunes, K. Yagi, and F. Pretorius, Phys. Rev. D **94**, 084002 (2016).
[17] A. Ghosh *et al.*, Phys. Rev. D **94**, 021101 (2016).

[18] K. G. Arun, B. R. Iyer, M. S. S. Qusailah, and B. S. Sathyaprakash, Classical Quantum Gravity **23**, L37 (2006).
[19] M. Isi, M. Giesler, W. M. Farr, M. A. Scheel, and S. A. Teukolsky, Phys. Rev. Lett. **123**, 111102 (2019).
[20] M. Isi, M. Pitkin, and A. J. Weinstein, Phys. Rev. D **96**, 042001 (2017).
[21] N. V. Krishnendu, K. G. Arun, and C. K. Mishra, Phys. Rev. Lett. **119**, 091101 (2017).
[22] S. Mirshekari, N. Yunes, and C. M. Will, Phys. Rev. D **85**, 024041 (2012).
[23] A. Vijaykumar, S. J. Kapadia, and P. Ajith, Phys. Rev. Lett. **126**, 141104 (2021).
[24] R. Niu, T. Zhu, and W. Zhao, J. Cosmol. Astropart. Phys. 12 (2022) 011.
[25] J. Zhao, L. Shao, Z. Cao, and B.-Q. Ma, Phys. Rev. D **100**, 064034 (2019).
[26] M. Okounkova, W. M. Farr, M. Isi, and L. C. Stein, Phys. Rev. D **106**, 044067 (2022).
[27] L. Jenks, K. Yagi, and S. Alexander, Phys. Rev. D **102**, 084022 (2020).
[28] T. Zhu, W. Zhao, and A. Wang, Phys. Rev. D **107**, 044051 (2023).
[29] Q. Wu, T. Zhu, R. Niu, W. Zhao, and A. Wang, Phys. Rev. D **105**, 024035 (2022).
[30] Y.-F. Wang, S. M. Brown, L. Shao, and W. Zhao, Phys. Rev. D **106**, 084005 (2022).
[31] Y.-F. Wang, R. Niu, T. Zhu, and W. Zhao, Astrophys. J. **908**, 58 (2021).
[32] L. Haegel, K. O'Neal-Ault, Q. G. Bailey, J. D. Tasson, M. Bloom, and L. Shao, Phys. Rev. D **107**, 064031 (2023).
[33] C. Gong, T. Zhu, R. Niu, Q. Wu, J.-L. Cui, X. Zhang, W. Zhao, and A. Wang, Phys. Rev. D **105**, 044034 (2022).
[34] Y. Du, S. Tahura, D. Vaman, and K. Yagi, Phys. Rev. D **103**, 044031 (2021).
[35] P. Kanti, N. E. Mavromatos, J. Rizos, K. Tamvakis, and E. Winstanley, Phys. Rev. D **54**, 5049 (1996).
[36] T. Torii, H. Yajima, and K.-i. Maeda, Phys. Rev. D **55**, 739 (1997).
[37] S. Nojiri, S. D. Odintsov, and M. Sasaki, Phys. Rev. D **71**, 123509 (2005).
[38] K. Yagi, Phys. Rev. D **86**, 081504 (2012).
[39] E. Berti *et al.*, Classical Quantum Gravity **32**, 243001 (2015).
[40] K. Yagi, L. C. Stein, N. Yunes, and T. Tanaka, Phys. Rev. D **85**, 064022 (2012); **93**, 029902(E) (2016).
[41] S. Tahura and K. Yagi, Phys. Rev. D **98**, 084042 (2018); **101**, 109902(E) (2020).
[42] B. Shiralilou, T. Hinderer, S. Nissanke, N. Ortiz, and H. Witek, Phys. Rev. D **103**, L121503 (2021).
[43] B. Shiralilou, T. Hinderer, S. M. Nissanke, N. Ortiz, and H. Witek, Classical Quantum Gravity **39**, 035002 (2022).
[44] F.-L. Julié, V. Baibhav, E. Berti, and A. Buonanno, Phys. Rev. D **107**, 104044 (2023).
[45] I. van Gemeren, B. Shiralilou, and T. Hinderer, Phys. Rev. D **108**, 024026 (2023).
[46] S. Tahura, K. Yagi, and Z. Carson, Phys. Rev. D **100**, 104001 (2019).
[47] R. Nair, S. Perkins, H. O. Silva, and N. Yunes, Phys. Rev. Lett. **123**, 191101 (2019).
[48] C. Shi, M. Ji, J.-d. Zhang, and J. Mei, Phys. Rev. D **108**, 024030 (2023).
[49] Z. Lyu, N. Jiang, and K. Yagi, Phys. Rev. D **105**, 064001 (2022).
[50] S. Mezzasoma and N. Yunes, Phys. Rev. D **106**, 024026 (2022).
[51] M. Okounkova, L. C. Stein, M. A. Scheel, and S. A. Teukolsky, Phys. Rev. D **100**, 104026 (2019).
[52] M. Okounkova, L. C. Stein, J. Moxon, M. A. Scheel, and S. A. Teukolsky, Phys. Rev. D **101**, 104016 (2020).
[53] M. Okounkova, Phys. Rev. D **102**, 084046 (2020).
[54] V. Cardoso, M. Kimura, A. Maselli, E. Berti, C. F. B. Macedo, and R. McManus, Phys. Rev. D **99**, 104077 (2019).
[55] R. McManus, E. Berti, C. F. B. Macedo, M. Kimura, A. Maselli, and V. Cardoso, Phys. Rev. D **100**, 044061 (2019).
[56] V. Baibhav, M. H.-Y. Cheung, E. Berti, V. Cardoso, G. Carullo, R. Cotesta, W. Del Pozzo, and F. Duque, arXiv:2302.03050.
[57] J. Bao, C. Shi, H. Wang, J.-d. Zhang, Y. Hu, J. Mei, and J. Luo, Phys. Rev. D **100**, 084024 (2019).
[58] K. Glampedakis, G. Pappas, H. O. Silva, and E. Berti, Phys. Rev. D **96**, 064054 (2017).
[59] J. L. Blázquez-Salcedo, C. F. B. Macedo, V. Cardoso, V. Ferrari, L. Gualtieri, F. S. Khoo, J. Kunz, and P. Pani, Phys. Rev. D **94**, 104024 (2016).
[60] Z. Carson and K. Yagi, Classical Quantum Gravity **37**, 215007 (2020).
[61] Z. Carson and K. Yagi, Phys. Rev. D **101**, 104030 (2020).
[62] G. S. Bonilla, P. Kumar, and S. A. Teukolsky, Phys. Rev. D **107**, 024015 (2023).
[63] S. Husa, S. Khan, M. Hannam, M. Pürrer, F. Ohme, X. Jiménez Forteza, and A. Bohé, Phys. Rev. D **93**, 044006 (2016).
[64] S. Khan, S. Husa, M. Hannam, F. Ohme, M. Pürrer, X. Jiménez Forteza, and A. Bohé, Phys. Rev. D **93**, 044007 (2016).
[65] C. García-Quirós, M. Colleoni, S. Husa, H. Estellés, G. Pratten, A. Ramos-Buades, M. Mateu-Lucena, and R. Jaume, Phys. Rev. D **102**, 064002 (2020).
[66] L. Blanchet, Living Rev. Relativity **17**, 2 (2014).
[67] N. Yunes, F. Pretorius, and D. Spergel, Phys. Rev. D **81**, 064018 (2010).
[68] M. Cabero, A. B. Nielsen, A. P. Lundgren, and C. D. Capano, Phys. Rev. D **95**, 064016 (2017).
[69] L. S. Finn, Phys. Rev. D **46**, 5236 (1992).
[70] C. M. Biwer, C. D. Capano, S. De, M. Cabero, D. A. Brown, A. H. Nitz, and V. Raymond, Publ. Astron. Soc. Pac. **131**, 024503 (2019).
[71] D. Foreman-Mackey, D. W. Hogg, D. Lang, and J. Goodman, Publ. Astron. Soc. Pac. **125**, 306 (2013).
[72] The LIGO Scientific Collaboration, Virgo Collaboration, and KAGRA Collaboration, arXiv:2111.03606.